

Mechanical fault detection in induction motor drives through stator current monitoring - Theory and application examples

Martin Blödt
Siemens AG
Germany

Pierre Granjon and Bertrand Raison
Grenoble-INP
France

Jérémi Regnier
INP Toulouse
France

1. Introduction

1.1 General Introduction

In a wide variety of industrial applications, an increasing demand exists to improve the reliability and availability of electrical systems. Popular examples include systems in aircraft, electric railway traction, power plant cooling or industrial production lines. A sudden failure of a system in these examples may lead to cost expensive downtime, damage to surrounding equipment or even danger to humans. Monitoring and failure detection improve the reliability and availability of an existing system. Since various failures degrade relatively slowly, there is a potential for fault detection followed by corrective maintenance at an early stage. This avoids the sudden, total system failure which can have serious consequences.

Electric machines are a key element in many electrical systems. Amongst all types of electric motors, induction motors are a frequent example due to their simplicity of construction, robustness and high efficiency. Common failures occurring in electrical drives can be roughly classified into:

Electrical faults: stator winding short circuit, broken rotor bar, broken end-ring, inverter failure

Mechanical faults: rotor eccentricity, bearing faults, shaft misalignment, load faults (unbalance, gearbox fault or general failure in the load part of the drive)

A reliability survey on large electric motors (>200 HP) revealed that most failures are due to bearing ($\approx 44\%$) and winding faults ($\approx 26\%$) (IEEE motor reliability working group (1985a))

(Engelmann & Middendorf (1995)). Similar results were obtained in an EPRI (Electric Power Research Institute) sponsored survey (Albrecht et al. (1987)). These studies concerned only the electric motor and not the whole drive including the load, but they show that mechanical fault detection is of great concern in electric drives.

A growing number of induction motors operates in variable speed drives. In this case, the motor is not directly connected to the power grid but supplied by an inverter. The inverter provides voltage of variable amplitude and frequency in order to vary the mechanical speed. Hence, this work addresses the problem of condition monitoring of mechanical faults in variable speed induction motor drives. A signal based approach is chosen i.e. the fault detection and diagnosis are only based on processing and analysis of measured signals and not on real-time models.

1.2 Motor Current Signature Analysis

A common approach for monitoring mechanical failures is vibration monitoring. Due to the nature of mechanical faults, their effect is most straightforward on the vibrations of the affected component. Since vibrations lead to acoustic noise, noise monitoring is also a possible approach. However, these methods are expensive since they require costly additional transducers. Their use only makes sense in case of large machines or highly critical applications. A cost effective alternative is stator current based monitoring since a current measurement is easy to implement. Moreover, current measurements are already available in many drives for control or protection purposes. However, the effects of mechanical failures on the motor stator current are complex to analyze. Therefore, stator current based monitoring is undoubtedly more difficult than vibration monitoring.

Another advantage of current based monitoring over vibration analysis is the limited number of necessary sensors. An electrical drive can be a complex and extended mechanical system. For complete monitoring, a large number of vibration transducers must be placed on the different system components that are likely to fail e.g. bearings, gearboxes, stator frame, load. However, a severe mechanical problem in any component influences necessarily the electric machine through load torque and shaft speed. This signifies that the motor can be considered as a type of intermediate transducer where various fault effects converge together. This strongly limits the number of necessary sensors. However, since numerous fault effects come together, fault diagnosis and discrimination become more difficult or sometimes even impossible.

A literature survey showed a lack of analytical models that account for the mechanical fault effect on the stator current. Most authors simply give expressions of additional frequencies but no precise stator current signal model. In various works, numerical machine models accounting for the fault are used. However, they do not provide analytical stator current expressions which are important for the choice of suitable signal analysis and detection strategies.

The most widely used method for stator current processing in this context is spectrum estimation. In general, the stator current power spectral density is estimated using Fourier transform based techniques such as the periodogram. These methods require stationary signals i.e. they are inappropriate when frequencies vary with respect to time such as during speed transients. Advanced methods for non-stationary signal analysis are required.

The organization of the present work is the following. Section 2 analyses the effects of load torque oscillations and dynamic eccentricity on the stator current. In section 3, suitable signal processing methods for stator current analysis are introduced. Experimental results under laboratory conditions are presented in section 4. Section 5 examines the detection of misalign-

ment faults in electric winches including analysis of experimental data from a real winch. Bearing faults are investigated apart in section 6 from a theoretical and practical point of view since they can introduce particular eccentricities and load torque oscillations.

2. Theoretical study of mechanical fault effects on stator current

The key assumption for the development of the theoretical models is that mechanical faults mainly produce two effects on induction machines: additional load torque oscillations at characteristic frequencies and/or airgap eccentricity.

Load torque oscillations can be caused by the following faults:

- load unbalance (not necessarily a fault but can also be inherent to the load type)
- shaft misalignment
- gearbox fault e.g. broken tooth
- bearing faults

Airgap eccentricity i.e. a non-uniform airgap can be for example the consequence of bearing wear or bearing failure, bad motor assembly with rotor unbalance or a rotor which is not perfectly centered. In general, eccentricity will be a sign for a mechanical problem within the electric motor whereas load torque oscillations point to a fault that is located outside of the motor.

The method used to study the influence of the periodic load torque variation and the rotor eccentricity on the stator current is the magnetomotive force (MMF) and permeance wave approach (Yang (1981)) (Timár (1989)) (Heller & Hamata (1977)). This approach is traditionally used for the calculation of the magnetic airgap field with respect to rotor and stator slotting or static and dynamic eccentricity (Cameron & Thomson (1986)) (Dorrell et al. (1997)).

First, the rotor and stator MMF are calculated which are directly related to the current flowing in the windings. The second important quantity is the airgap permeance Λ which is directly proportional to the inverse of the airgap length g . The magnetic field in the airgap can then be determined by multiplying the permeance by the sum of rotor and stator MMFs. The equivalent magnetic flux in one phase is obtained by integration of the magnetic field in each turn of the phase winding. The induced phase voltage, related to the current by the stator voltage equation, is then deduced from the magnetic flux.

As this work also considers variable speed drives, the supply frequency f_s and the characteristic fault frequency f_c may vary. Note that f_c can be for example the time-varying rotational frequency f_r . The theoretical stator current analysis during transients, however, is identical to the steady state if relatively slow frequency variations of f_s and f_c are considered.

2.1 Load torque oscillations

The influence of load torque oscillations on the stator current has been published for a general case by the authors in (Blödt, Chabert, Regnier & Faucher (2006)) (Blödt (2006)). The development will be shortly resumed in the following.

2.1.1 Effect on Rotor and Stator MMF

Under a mechanical fault, the load torque as a function of time is modeled by a constant component Γ_{const} and an additional component varying at the characteristic frequency f_c , depending on the fault type. It can be for example the rotational frequency f_r with load unbalance or a particular gearbox frequency in case of a gearbox fault. The first term of the variable

component Fourier series is a cosine with frequency f_c . For the sake of clarity and since they are usually of smaller amplitude, higher order terms at kf_c are neglected in the following and only the fundamental term is considered. The load torque can therefore be described by:

$$\Gamma_{load}(t) = \Gamma_{const} + \Gamma_c \cos(\omega_c t) \tag{1}$$

where Γ_c is the amplitude of the load torque oscillation and $\omega_c = 2\pi f_c$. The machine mechanical equation relates the torque oscillation to the motor speed ω_r and to the mechanical rotor position θ_r as follows:

$$\sum \Gamma(t) = \Gamma_{motor} - \Gamma_{load}(t) = J \frac{d\omega_r}{dt} = J \frac{d^2\theta_r}{dt^2} \tag{2}$$

where Γ_{motor} is the constant electromagnetic torque produced by the machine, J is the total inertia of the machine and the load.

After integrating twice, $\theta_r(t)$ is obtained as:

$$\theta_r(t) = \int_{t_0}^t \omega_r(\tau) d\tau = \frac{\Gamma_c}{J\omega_c^2} \cos(\omega_c t) + \omega_{r0}t \tag{3}$$

where ω_{r0} is the constant part of the motor speed. This equation shows that in contrast to the healthy machine where $\theta_r(t) = \omega_{r0}t$, oscillations at the characteristic frequencies are present on the mechanical rotor position.

The oscillations of the mechanical rotor position θ_r act on the rotor MMF. In a healthy state without faults, the fundamental rotor MMF in the rotor reference frame (R) is a wave with p pole pairs and frequency $s f_s$, given by:

$$F_r^{(R)}(\theta', t) = F_r \cos(p\theta' - s\omega_s t) \tag{4}$$

where θ' is the mechanical angle in the rotor reference frame (R) and s is the motor slip. Higher order space and time harmonics are neglected.

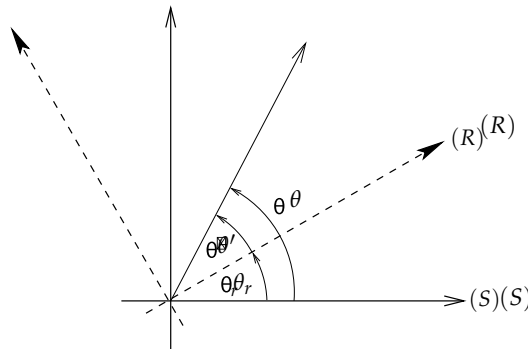


Fig. 1. Stator (S) and rotor (R) reference frame

Figure 1 illustrates the transformation between the rotor and stator reference frame, defined by $\theta = \theta' + \theta_r$. Using (3), this leads to:

$$\theta' = \theta - \omega_{r0}t - \frac{\Gamma_c}{J\omega_c^2} \cos(\omega_c t) \tag{5}$$

Thus, the rotor MMF given in (4) can be transformed to the stationary stator reference frame using (5) and the relation $\omega_{r0} = \omega_s(1 - s)/p$:

$$F_r(\theta, t) = F_r \cos(p\theta - \omega_s t - \beta \cos(\omega_c t)) \tag{6}$$

with:

$$\beta = p \frac{\Gamma_c}{J\omega_c^2} \tag{7}$$

Equation (6) clearly shows that the load torque oscillations at frequency f_c lead to a phase modulation of the rotor MMF in the stator reference frame. This phase modulation is characterized by the introduction of the term $\beta \cos(\omega_c t)$ in the phase of the MMF wave. The parameter β is generally called the modulation index. For physically reasonable values J , Γ_c and ω_c , the approximation $\beta \ll 1$ holds in most cases.

The fault has no direct effect on the stator MMF and so it is considered to have the following form:

$$F_s(\theta, t) = F_s \cos(p\theta - \omega_s t - \varphi_s) \tag{8}$$

φ_s is the initial phase difference between rotor and stator MMF. As in the case of the rotor MMF, only the fundamental space and time harmonic is taken into account; higher order space and time harmonics are neglected.

2.1.2 Effect on Flux Density and Stator Current

The airgap flux density $B(\theta, t)$ is the product of total MMF and airgap permeance Λ . The airgap permeance is supposed to be constant because slotting effects and eccentricity are not taken into account for the sake of clarity and simplicity.

$$\begin{aligned} B(\theta, t) &= [F_s(\theta, t) + F_r(\theta, t)] \Lambda \\ &= B_s \cos(p\theta - \omega_s t - \varphi_s) \\ &\quad + B_r \cos(p\theta - \omega_s t - \beta \cos(\omega_c t)) \end{aligned} \tag{9}$$

The phase modulation of the flux density $B(\theta, t)$ exists for the flux $\Phi(t)$ itself, as $\Phi(t)$ is obtained by simple integration of $B(\theta, t)$ with respect to the winding structure. The winding structure has only an influence on the amplitudes of the flux harmonic components, not on their frequencies. Therefore, $\Phi(t)$ in an arbitrary phase can be expressed in a general form:

$$\Phi(t) = \Phi_s \cos(\omega_s t + \varphi_s) + \Phi_r \cos(\omega_s t + \beta \cos(\omega_c t)) \tag{10}$$

The relation between the flux and the stator current in a considered phase is given by the stator voltage equation:

$$V(t) = R_s I(t) + \frac{d\Phi(t)}{dt} \tag{11}$$

With $V(t)$ imposed by the voltage source, the resulting stator current will be in a linear relation to the time derivative of the phase flux $\Phi(t)$ and will have an equivalent frequency content. Differentiating (10) leads to:

$$\begin{aligned} \frac{d}{dt} \Phi(t) &= -\omega_s \Phi_s \sin(\omega_s t + \varphi_s) \\ &\quad - \omega_s \Phi_r \sin(\omega_s t + \beta \cos(\omega_c t)) \\ &\quad + \omega_c \beta \Phi_r \sin(\omega_s t + \beta \cos(\omega_c t)) \sin(\omega_c t) \end{aligned} \tag{12}$$

The amplitude of the last term is smaller than that of the other terms because $\beta \ll 1$. Thus, the last term in (12) will be neglected in the following.

As a consequence, the stator current in an arbitrary phase can be expressed in a general form:

$$\begin{aligned} I_{i0}(t) &= i_{st}(t) + i_{rt}(t) \\ &= I_{st} \sin(\omega_s t + \varphi_s) + I_{rt} \sin(\omega_s t + \beta \cos(\omega_c t)) \end{aligned} \quad (13)$$

Therefore the stator current $I(t)$ can be considered as the sum of two components. The term $i_{st}(t)$ results from the stator MMF and it is not modulated. The term $i_{rt}(t)$, which is a direct consequence of the rotor MMF shows the phase modulation due to the considered load torque oscillations. The healthy case is obtained for $\beta = 0$.

In this study, the time harmonics of rotor MMF and the non-uniform airgap permeance have not been considered. However, the harmonics of supply frequency f_s and the rotor slot harmonics will theoretically show the same phase modulation as the fundamental component.

2.2 Airgap Eccentricity

Airgap eccentricity leads to an airgap length that is no longer constant with respect to the stator circumference angle θ and/or time. In general, three types of airgap eccentricity can be distinguished (see Fig. 2):

Static eccentricity: The rotor geometrical and rotational centers are identical, but different from the stator center. The point of minimal airgap length is stationary with respect to the stator.

Dynamic eccentricity: The rotor geometrical center differs from the rotational center. The rotational center is identical with the stator geometrical center. The point of minimal airgap length is moving with respect to the stator.

Mixed eccentricity: The two effects are combined. The rotor geometrical and rotational center as well as the stator geometrical center are different.

In the following theoretical development, static and dynamic eccentricity will be considered.

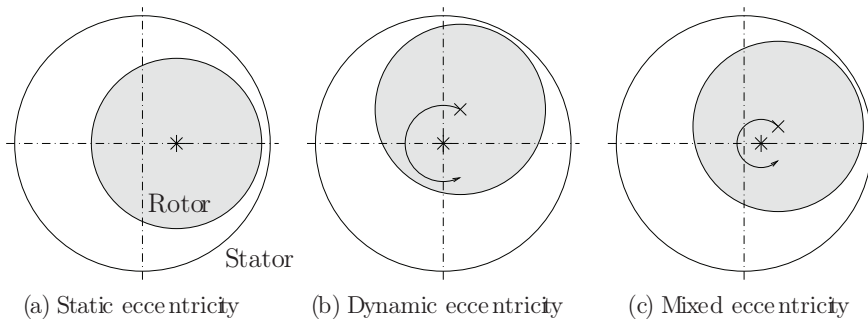


Fig. 2. Schematic representation of static, dynamic and mixed eccentricity. \times denotes the rotor geometrical center, $*$ the rotor rotational center

The airgap length $g(\theta, t)$ can be approximated for a small airgap and low levels of static or dynamic eccentricity by the following expression (Dorrell et al. (1997)):

$$\begin{aligned} g_{se}(\theta, t) &\approx g_0(1 - \delta_s \cos(\theta)) \\ g_{de}(\theta, t) &\approx g_0(1 - \delta_d \cos(\theta - \omega_r t)) \end{aligned} \quad (14)$$

where δ_s, δ_d denote the relative degrees of static or dynamic eccentricity and g_0 the mean airgap length without eccentricity. Note that static eccentricity can be considered as a special case of dynamic eccentricity since $g_{se}(\theta, t)$ corresponds to $g_{de}(\theta, t)$ with $\omega_r = 0$, i.e. the point of minimum airgap length is stationary. Since dynamic eccentricity is more general, it will mainly be considered in the following.

The airgap permeance $\Lambda(\theta, t)$ is obtained as the inverse of $g(\theta, t)$ multiplied by the permeability of free space μ_0 . Following a classical approach, the permeance is written as a Fourier series (Cameron & Thomson (1986)):

$$\Lambda_{de}(\theta, t) = \Lambda_0 + \sum_{i_{ecc}=1}^{\infty} \Lambda_{i_{ecc}} \cos(i_{ecc}\theta - i_{ecc}\omega_r t) \tag{15}$$

where $\Lambda_0 = \mu_0/g_0$ is the permeance without eccentricity. The higher order coefficients of the Fourier series can be written as (Cameron & Thomson (1986)):

$$\Lambda_{i_{ecc}} = \frac{2\mu_0(1 - \sqrt{1 - \delta^2})^{i_{ecc}}}{g_0\delta_d^{i_{ecc}}\sqrt{1 - \delta^2}} \tag{16}$$

Dorrell has shown in (Dorrell (1996)) that the coefficients with $i_{ecc} \geq 2$ are rather small for $\delta_d < 40\%$. For the sake of simplicity, they are neglected in the following considerations.

The airgap flux density is the product of permeance with the magnetomotive force (MMF). The total fundamental MMF wave can be written as:

$$F_{tot}(\theta, t) = F_1 \cos(p\theta - \omega_s t - \varphi_t) \tag{17}$$

with φ_t the initial phase. Hence, the flux density in presence of dynamic eccentricity is:

$$B_{de}(\theta, t) \approx B_1 \left[1 + 2\frac{\Lambda_1}{\Lambda_0} \cos(\theta - \omega_r t) \right] \cos(p\theta - \omega_s t - \varphi_t) \tag{18}$$

with $B_1 = \Lambda_0 F_1$

The fraction $2\Lambda_1/\Lambda_0$ equals approximately δ_d for small levels of eccentricity. The airgap flux density can therefore be written as:

$$B_{de}(\theta, t) = B_1 [1 + \delta_d \cos(\theta - \omega_r t)] \cos(p\theta - \omega_s t - \varphi_t) \tag{19}$$

This equation shows the fundamental effect of dynamic eccentricity on the airgap magnetic flux density : the modified airgap permeance causes an amplitude modulation of the fundamental flux density wave with respect to time and space. The AM modulation index is approximately the degree of dynamic eccentricity δ .

In case of static eccentricity, the fundamental flux density expresses as:

$$B_{se}(\theta, t) = B_1 [1 + \delta_s \cos(\theta)] \cos(p\theta - \omega_s t - \varphi_t) \tag{20}$$

which shows that static eccentricity leads only to flux density AM with respect to space.

Consequently, the amplitude modulation can also be found on the stator current $I(t)$ (see section 2.1.2) that is expressed as follows in case of dynamic eccentricity:

$$I_{de}(t) = I_1 [1 + \alpha \cos(\omega_r t)] \cos(\omega_s t - \varphi_i) \tag{21}$$

In this expression, I_1 denotes the amplitude of the stator current fundamental component, α the AM modulation index which is proportional to the degree of dynamic eccentricity δ_d . Static eccentricity does not lead to frequencies different from ω_s since the corresponding additional flux density waves are also at the supply pulsation ω_s . It can be concluded that theoretically, pure static eccentricity cannot be detected by stator current analysis.

3. Signal processing tools for fault detection and diagnosis

The previous section has shown that load torque oscillations cause a phase modulation on one stator current component according to (13). On the other hand, dynamic airgap eccentricity leads to amplitude modulation of the stator current (see (21)). In this section, signal processing methods for detection of both modulation types in the stator current will be presented and discussed.

In order to simplify calculations, all signals will be considered in their complex form, the so-called analytical signal (Boashash (2003)) (Flandrin (1999)). The analytical signal $z(t)$ is related to the real signal $x(t)$ via the Hilbert Transform $H\{\cdot\}$:

$$z(t) = x(t) + jH\{x(t)\} \quad (22)$$

The analytical signal contains the same information as the real signal but its Fourier transform is zero at negative frequencies.

3.1 Power Spectral Density

3.1.1 Definition

The classical method for signal analysis in the frequency domain is the estimation of the Power Spectral Density (PSD) based on the discrete Fourier transform of the signal $x[n]$. The PSD indicates the distribution of signal energy with respect to the frequency. The common estimation method for the PSD is the periodogram $P_{xx}(f)$ (Kay (1988)), defined as the square of the N -point Fourier transform divided by N :

$$P_{xx}(f) = \frac{1}{N} \left| \sum_{n=0}^{N-1} x(n) e^{-j2\pi f n} \right|^2 \quad (23)$$

3.1.2 Application

The PSD represents the basic signal analysis tool for stationary signals i.e. it can be used in case of a constant or quasi-constant supply frequency during the observation interval.

The absolute value of the Fourier transform $|I(f)|$ of the stator current PM signal (13) is obtained as follows (see Blödt, Chabert, Regnier & Faucher (2006) for details):

$$\begin{aligned} |I_{to}(f)| &= (I_{st} + I_{rt} J_0(\beta)) \delta(f - f_s) \\ &+ I_{rt} \sum_{n=-\infty}^{+\infty} J_n(\beta) \delta(f - (f_s \pm n f_c)) \end{aligned} \quad (24)$$

where J_n denotes the n -th order Bessel function of the first kind and $\delta(f)$ is the Dirac delta function. For small modulation index β , the Bessel functions of order $n \geq 2$ are very small and may be neglected (the so-called narrowband approximation). It becomes clear through this expression that the fault leads to sideband components of the fundamental at $f_s \pm n f_c$. When the modulation index β is small, only the first order sidebands at $f_s \pm f_c$ will be visible and their amplitudes will be approximately $J_1(\beta) I_{rt} \approx 0.5 \beta I_{rt}$.

The Fourier transform magnitude of the AM stator current signal according to (21) is:

$$|I_{de}(f)| = I_1 \delta(f - f_s) + \frac{1}{2} \alpha I_1 \delta(f - (f_s \pm f_c)) \quad (25)$$

The amplitude modulation leads to two sideband components at $f_s \pm f_c$ with equal amplitude $\alpha I_1 / 2$. Therefore, the spectral signature of the AM and PM signal is identical if the modulation

frequency is equal and the PM modulation index is small. This can be the case when e.g. load unbalance and dynamic rotor eccentricity are considered as faults.

It can be concluded that the PSD is a simple analysis tool for stationary drive conditions. It is not suitable for analysis when the drive speed is varying. Another drawback is that PM and AM cannot be clearly distinguished.

3.2 Instantaneous Frequency

3.2.1 Definition

For a complex monocomponent signal $z(t) = a(t)e^{j\varphi(t)}$, the instantaneous frequency $f_i(t)$ is defined by (Boashash (2003)):

$$f_i(t) = \frac{1}{2\pi} \frac{d}{dt} \varphi(t) \tag{26}$$

where $\varphi(t)$ is the instantaneous phase and $a(t)$ the instantaneous amplitude of the analytical signal $z(t)$.

3.2.2 Application

The instantaneous frequency (IF) of a monocomponent phase modulated signal can be calculated using the definition (26). For the phase modulated stator current component $i_{rt}(t)$ (see second term of equation (13)), it can be expressed as:

$$f_{i,i_{rt}}(t) = f_s - f_c \beta \sin(\omega_c t) \tag{27}$$

The fault has therefore a direct effect on the IF of the stator current component $i_{rt}(t)$. In the healthy case, its IF is constant; in the faulty case, a time varying component with frequency f_c appears.

If the complex multicomponent PM signal according to (13) is considered, the calculation of its IF leads to the following expression:

$$f_{i,I}(t) = f_s - f_c \beta \sin(\omega_c t) \frac{1}{1 + a(t)} \tag{28}$$

with

$$a(t) = \frac{I_{st}^2 + I_{st} I_{rt} \cos(\beta \cos(\omega_c t) - \varphi_s)}{I_{rt}^2 + I_{st} I_{rt} \cos(\beta \cos(\omega_c t) - \varphi_s)} \tag{29}$$

Using reasonable approximations, it can be shown that $1 / (1 + a(t))$ is composed of a constant component with only small oscillations. Hence, the IF of (13) may be approximated by:

$$f_{i,I}(t) \approx f_s - C f_c \beta \sin(\omega_c t) \tag{30}$$

where C is a constant, $C < 1$. Numerical evaluations confirm this approximation. It can therefore be concluded, that the multicomponent PM signal IF corresponding to the stator current also shows fault-related oscillations at f_c which may be used for detection.

The IF of an AM stator current signal according to (21) is simply a constant at frequency f_s . In contrast to the PM stator current signal, no time-variable component is present. The AM modulation index α is not reflected in the IF. Consequently, the stator current IF cannot be used for amplitude modulation detection i.e. airgap eccentricity related faults.

3.3 Wigner Distribution

The Wigner Distribution (WD) belongs to the class of time-frequency signal analysis tools. It provides a signal representation with respect to time and frequency which can be interpreted as a distribution of the signal energy.

3.3.1 Definition

The WD is defined as follows (Flandrin (1999)):

$$W_x(t, f) = \int_{-\infty}^{+\infty} x\left(t + \frac{\tau}{2}\right) x^*\left(t - \frac{\tau}{2}\right) e^{-j2\pi f\tau} d\tau \quad (31)$$

This formula can be seen as the Fourier transform of a kernel $K_x(\tau, t)$ with respect to the delay variable τ . The kernel is similar to an autocorrelation function.

An interesting property of the WD is its perfect concentration on the instantaneous frequency in the case of a linear frequency modulation. However, other types of modulations (e.g. in our case sinusoidal phase modulations) produce so-called inner interference terms in the distribution (Mecklenbräuker & Hlawatsch (1997)). Note that the interferences may however be used for detection purposes as it will be shown in the following.

Another important drawback of the distribution is its non-linearity due to the quadratic nature. When the sum of two signals is considered, so-called outer interference terms appear in the distribution at time instants or frequencies where there should not be any signal energy (Mecklenbräuker & Hlawatsch (1997)). The interference terms can be reduced by using e.g. the Pseudo Wigner Distribution which includes an additional smoothing window (see section 3.4).

3.3.2 Application

The stator current in the presence of load torque oscillations can be considered as the sum of a pure frequency and a phase modulated signal (see (13)). The detailed calculations of the stator current WD can be found in (Blödt, Chabert, Regnier & Faucher (2006)). The following approximate expression is obtained for small β :

$$\begin{aligned} W_{i_{pm}}(t, f) \approx & \left(I_{rt}^2 + I_{st}^2 \right) \delta(f - f_s) \\ & - I_{rt}^2 \beta \sin(\omega_c t) \delta\left(f - f_s - \frac{f_c}{2}\right) \\ & + I_{rt}^2 \beta \sin(\omega_c t) \delta\left(f - f_s + \frac{f_c}{2}\right) \end{aligned} \quad (32)$$

The WD of the PM stator current is therefore a central frequency at f_s with sidebands at $f_s \pm f_c/2$. These components have time-varying amplitudes at frequency f_c . It is important to note that the lower sideband has the opposed sign to the upper sideband for a given point in time i.e. a phase shift of π exists theoretically between the two sidebands.

The WD of the AM signal according to (21) is calculated in details in (Blödt, Regnier & Faucher (2006)). The following approximate expression is obtained for small modulation indices α :

$$W_{i_{am}}(t, f) \approx I_1^2 \delta(f - f_s) + \alpha \cos(\omega_r t) I_1^2 \delta\left(f - f_s \pm \frac{f_r}{2}\right) \quad (33)$$

The AM signature on the WD is therefore sidebands at $f_s \pm f_r/2$. The sidebands oscillate at shaft rotational frequency f_r , their amplitude is αI_1^2 . It should be noted that the signature is

similar to the PM signal but with the important difference that the upper and lower sideband oscillations have the same amplitudes for a given point in time i.e. they are in phase.

3.4 Illustration with Synthesized Signals

In order to validate the preceding theoretical considerations, the periodogram and WD of AM and PM signals are calculated numerically with synthesized signals. The signals are discrete versions of the continuous time signals in (13) and (21) with the following parameters: $I_{st} = I_{rt} = \sqrt{2}/2$, $I_1 = \sqrt{2}$, $\alpha = \beta = 0.1$, $\varphi_s = -\pi/8$, $f_s = 0.25$ and $f_c = f_r = 0.125$ normalized frequency. These parameters are coherent with a realistic application, apart from the strong modulation indices which are used for demonstration purposes. White zero-mean Gaussian noise is added with a signal to noise ration of 50 dB. The signal length is $N = 512$ samples.

First, the periodogram of both signals is calculated (see Fig. 3). Both spectra show the fundamental component with sidebands at $f_s \pm f_r$. The higher order sidebands of the PM signal are buried in the noise floor so that both spectral signatures are identical.

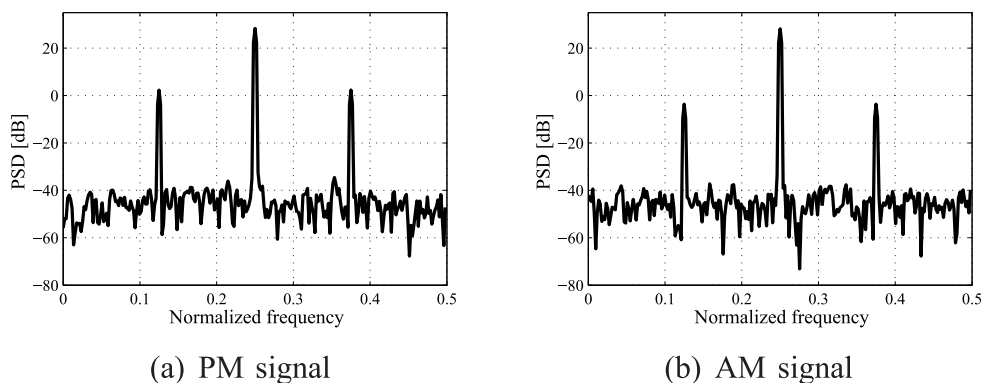


Fig. 3. Power spectral density of synthesized PM and AM signals.

The WD is often replaced in practical applications with the Pseudo Wigner Distribution (PWD). The PWD is a smoothed and windowed version of the WD, defined as follows: (Flandrin (1999)):

$$PW_x(t, f) = \int_{-\infty}^{+\infty} p(\tau) x\left(t + \frac{\tau}{2}\right) x^*\left(t - \frac{\tau}{2}\right) e^{-j2\pi f \tau} d\tau \quad (34)$$

where $p(\tau)$ is the smoothing window. In the following, a Hanning window of length $N/4$ is used. The time-frequency distributions are calculated using the Matlab® Time-Frequency Toolbox (Auger et al. (1995/1996)). The PWD of the PM and AM stator current signals is displayed in Fig. 4. A constant frequency at $f_s = 0.25$ is visible in each case. Sidebands resulting from modulation appear at $f_s \pm f_r/2$ in both cases. The zoom on the interference structure shows that the sidebands are oscillating at f_r . According to the theory, the sidebands are phase-shifted by approximately π in the PM case whereas they are in phase with the AM signal.

For illustrating the stator current IF analysis, a simulated transient stator current signal is used. The supply frequency $f_s(t)$ varies from 0.05 to 0.25 normalized frequency. The modulation frequency $f_c(t)$ is half the supply frequency. The IF of the transient PM and AM stator

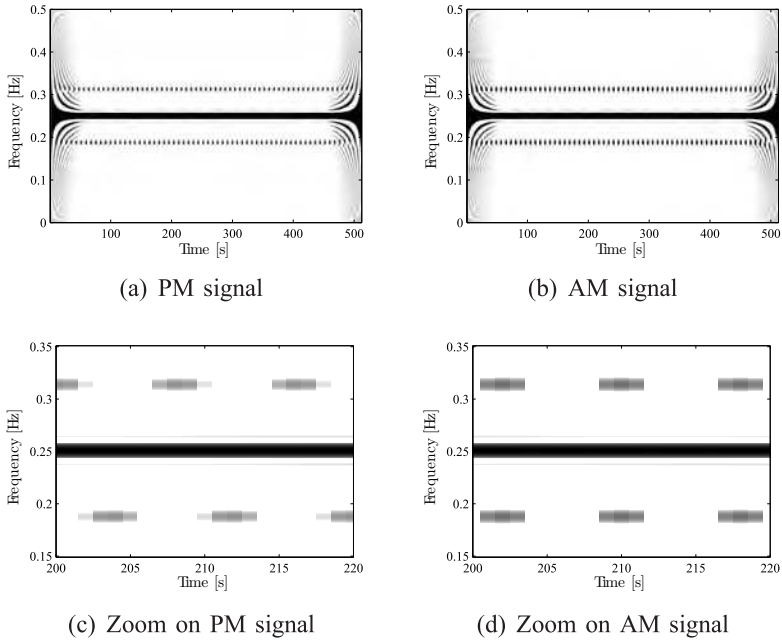


Fig. 4. Pseudo Wigner Distribution of synthesized PM and AM signals with zoom on interference structure.

current signal is shown in Fig. 5. The linear evolution of the supply frequency is clearly visible apart from border effects. With the PM signal, oscillations at varying fault frequency $f_c(t)$ can be recognized. In case of the AM signal, no oscillations are present. Further IF and PWD analysis with automatic extraction of fault indicators is described in (Blödt, Bonacci, Regnier, Chabert & Faucher (2008)).

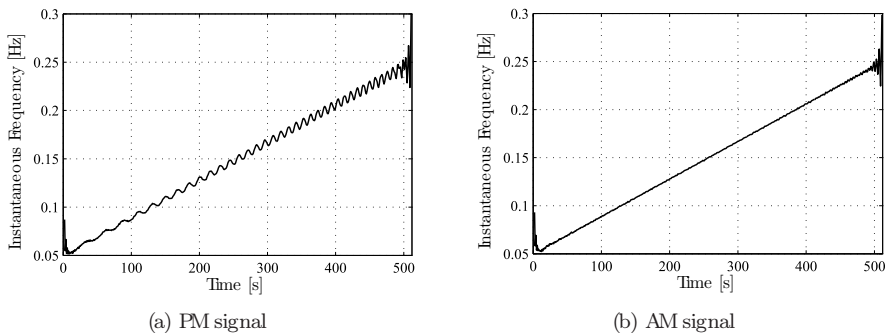


Fig. 5. Instantaneous frequency of simulated transient PM and AM signals.

3.5 Summary

Several signal processing methods suitable for the detection of mechanical faults by stator current analysis have been presented. Classical spectral analysis based on the PSD can give a first indication of a possible fault by an increase of sidebands at $f_s \pm f_r$. This method can only be applied in case of stationary signals without important variations of the supply frequency. The IF can be used to detect phase modulations since they lead to a time-varying IF. A global time-frequency signal analysis is possible using the WD or PWD where a characteristic interference structure appears in presence of the phase or amplitude modulations. The three methods have been illustrated with simulated signals.

4. Detection of dynamic airgap eccentricity and load torque oscillations under laboratory conditions

4.1 Experimental Setup

Laboratory tests have been performed on an experimental setup (see Fig.6) with a three phase, 400 V, 50 Hz, 5.5 kW Leroy Somer induction motor (motor A). The motor has $p = 2$ pole pairs and its nominal torque Γ_n is about 36 Nm. The machine is supplied by a standard industrial inverter operating in open-loop condition with a constant voltage to frequency ratio. The switching frequency is 3 kHz.

The load is a DC motor with separate, constant excitation connected to a resistor through a DC/DC buck converter. A standard PI controller regulates the DC motor armature current. Thus, using an appropriate current reference signal, a constant torque with a small additional oscillating component can be introduced. The sinusoidal oscillation is provided through a voltage controlled oscillator (VCO) linked to a speed sensor.

Since the produced load torque oscillations are not a realistic fault, load unbalance is also examined. Thereto, a mass is fixed on a disc mounted on the shaft. The torque oscillation produced by such a load unbalance is sinusoidal at shaft rotational frequency. With the chosen mass and distance, the torque oscillation amplitude is $\Gamma_c = 0.04$ Nm. If the motor bearings are healthy, the additional centrifugal forces created by the mass will not lead to airgap eccentricity.

A second induction motor with identical parameters has been modified to introduce dynamic airgap eccentricity (motor B). Therefore, the bearings have been replaced with bearings having a larger inner diameter. Then, eccentric fitting sleeves have been inserted between the shaft and the inner race. The obtained degree of dynamic eccentricity is approximately 40%.

Measured quantities in the experimental setup include the stator voltages and currents, torque and shaft speed. The signals are simultaneously acquired through a 24 bit data acquisition board at 25 kHz sampling frequency. Further signal processing is done off-line with Matlab®.

4.2 Stator Current Spectrum Analysis

For illustration purposes, the stator current spectral signatures of a machine with dynamic eccentricity (motor B) are compared to an operation with load torque oscillations at frequency $f_c = f_r$ (motor A). In Fig. 7 the current spectrum of a motor with 40% dynamic eccentricity is compared to an operation with load torque oscillations of amplitude $\Gamma_c=0.14$ Nm. This corresponds to only 0.4% of the nominal torque. The healthy motor spectrum is also displayed and the average load is 10% of nominal load during this test. The stator current spectra show identical fault signatures around the fundamental frequency i.e. an increasing amplitude of the peaks at $f_s \pm f_r \approx 25$ Hz and 75 Hz. This behavior is identical under different load conditions.

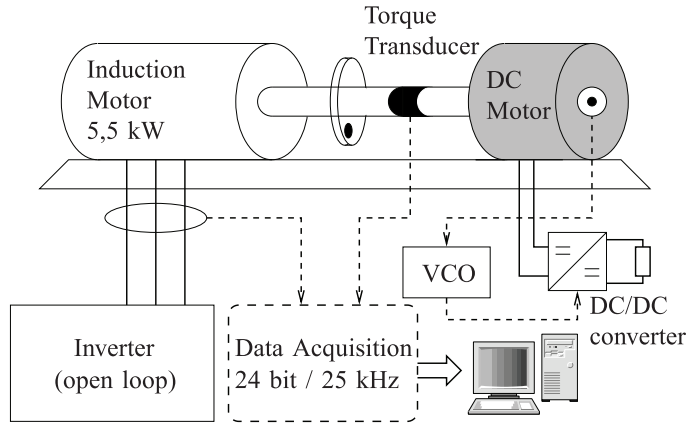


Fig. 6. Scheme of experimental setup

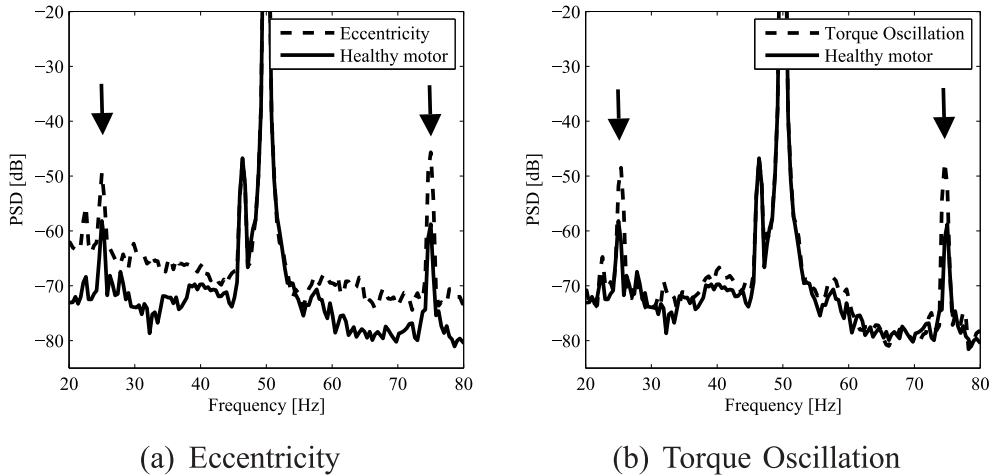


Fig. 7. Comparison of experimental motor stator current spectra: 40 % eccentricity (B) vs. healthy machine (A) and 0.14 Nm load torque oscillation (A) vs. healthy machine (A) at 10% average load.

The stator current with load unbalance is analyzed in Fig. 8. A small weight has been fixed on the disc on the shaft and the amplitude of the introduced torque oscillation is $\Gamma_c = 0.04$ Nm. The load unbalance as a realistic fault also leads to a rise in sideband amplitudes at $f_s \pm f_r$. These examples show that a monitoring strategy based on the spectral components $f_s \pm f_r$ can be used efficiently for detection purposes. In all three cases, these components show a considerable rise. However, this monitoring approach cannot distinguish between dynamic eccentricity and load torque oscillations.

In the following, transient stator current signals are also considered. They are obtained during motor startup between standstill and nominal supply frequency. The frequency sweep rate

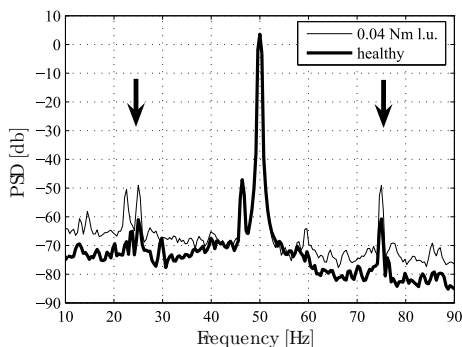


Fig. 8. PSD of stator current with load unbalance $\Gamma_c = 0.04$ Nm vs. healthy case

is 10 Hz per second i.e. the startup takes 5 seconds. For the following analysis, the transient between $f_s = 10$ Hz and 48 Hz is extracted. The PSD of a healthy and faulty transient signal are displayed in Fig. 9. This example illustrates that classic spectral estimation is not appropriate for transient signal analysis. The broad peak due to the time-varying supply frequency masks all other phenomena. The faulty and healthy case cannot be distinguished.

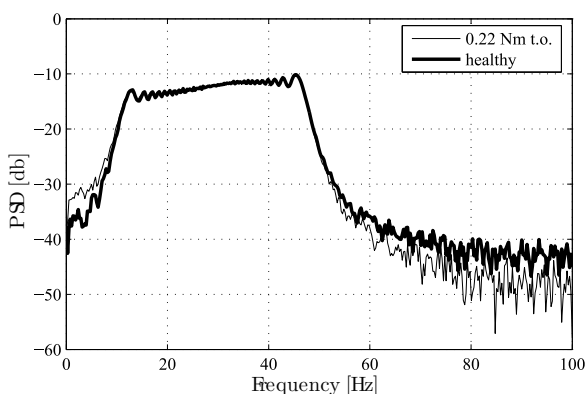


Fig. 9. PSD of stator current during speed transient with load torque oscillation $\Gamma_c = 0.22$ Nm vs. healthy case.

4.3 Stator Current Instantaneous Frequency Analysis

In this section, instantaneous frequency analysis will be applied to the stator current signals. The original signal has been lowpass filtered and downsampled to 200 Hz in order to remove high frequency content before time-frequency analysis. Only the information in a frequency range around the fundamental is conserved.

First, a transient stator current IF is shown in Fig. 10 for the healthy case and with a load torque oscillation $\Gamma_c = 0.5$ Nm. When load torque oscillations are present, the IF oscillations increase. The oscillation frequency is approximately half the supply frequency which corresponds to the shaft rotational frequency f_r .

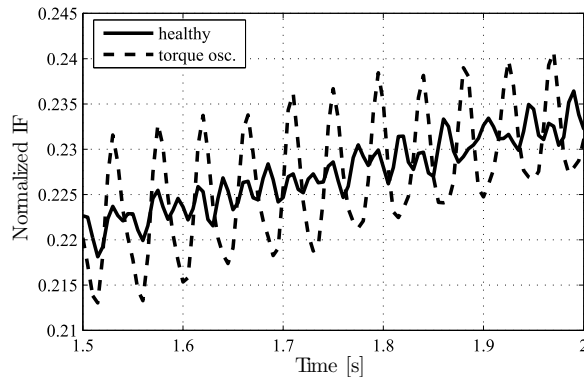


Fig. 10. Example of transient stator current IF with load torque oscillation ($\Gamma_c = 0.5 \text{ Nm}$) vs. healthy case, 25% load.

For further analysis, the IF spectrogram can be employed. The spectrogram is a time-frequency signal analysis based on sliding short time Fourier transforms. More information can be found in (Boashash (2003)) (Flandrin (1999)). The two spectrograms depicted in Fig. 11 analyze the stator current IF during a motor startup with a small oscillation of $\Gamma_c = 0.22 \text{ Nm}$ and 10% average load. Besides the strong DC level at 0 Hz in the spectrogram, time varying components can already be noticed in the healthy case (a). They correspond to the supply frequency $f_s(t)$ and its second harmonic. Comparing the spectrogram of the healthy IF to the one with load torque oscillations (b), a fault-related component at $f_r(t)$ becomes clearly visible. More information about IF analysis can be found in (Blödt (2006)).

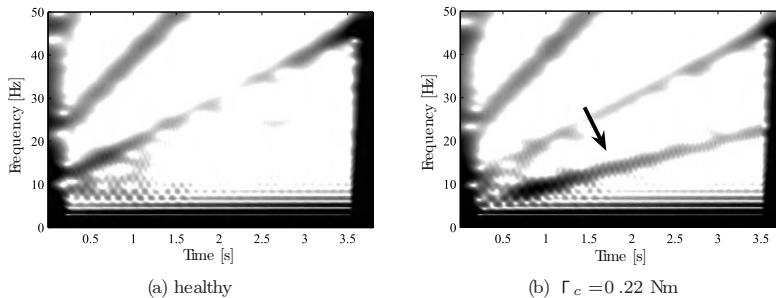


Fig. 11. Spectrogram of transient stator current IF with load torque oscillation $\Gamma_c = 0.22 \text{ Nm}$ vs. healthy case, 10% load.

4.4 Pseudo Wigner Distribution of Stator Current

The previously considered transient signals are also analyzed with the PWD. Figure 12 shows an example of the stator current PWD during a motor startup. Comparing the healthy case to 0.22 Nm load torque oscillations, the characteristic interference signature becomes visible around the time-varying fundamental frequency. Since the fault frequency is also time variable, the sideband location and their oscillation frequency depend on time (Blödt et al. (2005)).

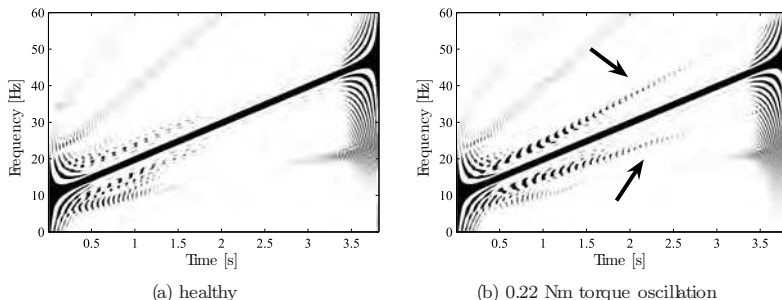


Fig. 12. PWD of transient stator current in healthy case and with load torque oscillation, 10% average load.

It is thereafter verified if dynamic eccentricity and load torque oscillations can be distinguished through the stator current PWD. The stator current PWDs with dynamic eccentricity and with 0.14 Nm load torque oscillation are shown in Fig. 13 for 10% average load. The characteristic fault signature is visible in both cases at $f_s \pm f_r/2 = 37.5$ Hz and 62.5 Hz. The phase shift between the upper and lower sideband seems closer to zero with eccentricity whereas with torque oscillations, it is closer to π . Nevertheless, it is difficult to determine the exact value from a visual analysis. However, the phase difference between the upper and lower sidebands can be automatically extracted from the PWD (see (Blödt, Regnier & Faucher (2006))). The result is about 125° with load torque oscillations and around 90° with dynamic eccentricity. These values differ from the theoretical ones (180° and 0° respectively) but this can be explained with load torque oscillations occurring as a consequence of dynamic eccentricity. A detailed discussion can be found in (Blödt, Regnier & Faucher (2006)). However, the phase shifts are sufficient to distinguish the two faults.

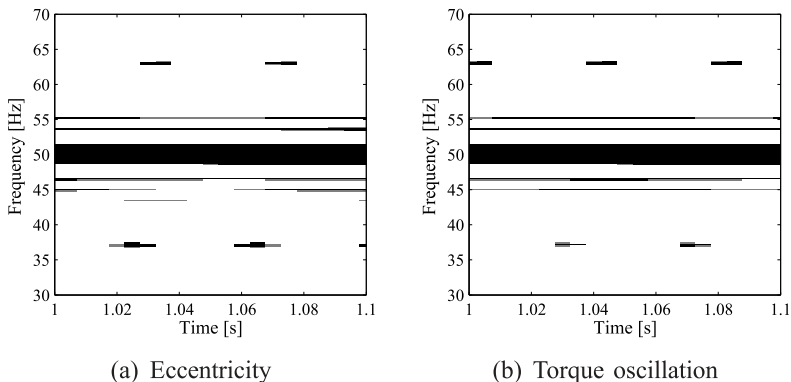


Fig. 13. Detail of stator current PWD with 40% dynamic eccentricity (B) and 0.14 Nm load torque oscillation (A) at small average load

Thank You for previewing this eBook

You can read the full version of this eBook in different formats:

- HTML (Free /Available to everyone)
- PDF / TXT (Available to V.I.P. members. Free Standard members can access up to 5 PDF/TXT eBooks per month each month)
- Epub & Mobipocket (Exclusive to V.I.P. members)

To download this full book, simply select the format you desire below

